Geophysical Research Letters

RESEARCH LETTER
10.1029/2019GL083670

Stepwise Weakening of the Pliocene Leeuwin Current

David De Vleeschouwer[1], Benjamin F. Petrick[2], and Alfredo Martínez-García[2]

[1]MARUM-Center for Marine Environmental Sciences, University of Bremen, Bremen, Germany, [2]Max-Planck-Institut für Chemie, Mainz, Germany

Key Points:
- LC has been active throughout the Pliocene, albeit with significant variations in intensity and scope
- Tectonic Indonesian Throughflow constriction caused a stepwise reduction in LC intensity 3.7 million years ago
- On orbital timescales, eustatic sea level and direct orbital forcing of wind patterns hampered or promoted the Pliocene LC

Supporting Information:
- Supporting Information S1

Correspondence to:
D. De Vleeschouwer,
ddevleeschouwer@marum.de

Citation:
De Vleeschouwer, D., Petrick, B. F., & Martínez-García, A. (2019). Stepwise weakening of the Pliocene Leeuwin Current. *Geophysical Research Letters*, *46*, 8310–8319. https://doi.org/10.1029/2019GL083670

Received 14 MAY 2019
Accepted 4 JUL 2019
Accepted article online 9 JUL 2019
Published online 22 JUL 2019

Abstract The Indonesian Throughflow (ITF) operates as an important link in global thermohaline circulation, and ITF variability probably modulated Pliocene climate change. Yet, whether ITF variability accounted for oceanographic change south of Northwest Cape remains controversial. Here, we present a multiproxy oceanographic reconstruction from the Perth Basin and reconstruct the Pliocene history of the Leeuwin Current (LC). We show that the LC was active throughout the Pliocene, albeit with fluctuations in intensity and scope. Three main factors controlled LC strength. First, a tectonic ITF reorganization caused an abrupt and permanent LC reduction at 3.7 Ma. On shorter timescales, eustatic sea level and direct orbital forcing of wind patterns hampered or promoted the LC. At 3.3 Ma, for instance, LC intensity plunged in response to a eustatic ITF restriction. Site U1459 then fell outside the extent of a weakened LC, and the latitudinal sea surface temperature gradient along West Australia doubled its steepness.

Plain Language Summary The Leeuwin Current (LC) transports warm, low-salinity, nutrient-deficient water poleward along Australia's west coast. The current is remarkable because eastern boundary currents usually flow equatorward (e.g., Benguela, California Current). The LC extends modern coral reef development to 29°S, but its geological history remains controversial. We use a sediment core (International Ocean Discovery Program Site U1459) from the Perth basin to reconstruct the Pliocene history of the LC. Based on variations in the multiproxy geochemical records of Site U1459 and comparison with contemporaneous sediment cores off northwest Australia, we show that poleward flowing warm waters reached the site throughout the Pliocene. The current's intensity exhibits a stepwise decline at 3.7 Ma though, in response to a tectonic reorganization around Indonesia, and a short-lived dramatic downturn during global glaciation event marine isotope stage M2 (3.3 Ma), in response to a sea level drop.

1. Introduction

The Indonesian Throughflow (ITF) connects the equatorial Pacific to the Indian Ocean and forms a crucial link in the global thermohaline conveyor. The ITF consists of numerous shallow currents that transport warm, low-salinity, nutrient-deficient water from the Indo-Pacific warm pool region into the Indian Ocean. Next, the warm water serves as a source for the South Equatorial Current, as well as for the Leeuwin Current (LC; Figure 1). The LC is a surface current that is up to ~300 m deep (Furue et al., 2017; Wijeratne et al., 2018; Woo & Pattiaratchi, 2008) and flows southward along the western coast of Australia. The LC is an eastern boundary current that meanders near the continental shelf break (Pearce, 1991; Smith et al., 1991) but differs from other eastern boundary currents in the fact that it flows poleward rather than equatorward. This implies that today's LC has to overcome the equatorward wind stress, Ekman-induced upwelling, and friction along the seafloor to maintain its southward flow over the continental shelf (Feng et al., 2007; Holloway, 1995; Pearce, 1991; Thompson et al., 2011; Waite et al., 2007; Weaver & Middleton, 1990; Wijeratne et al., 2018). An important driver for the LC is the steric height difference between low-density, low-salinity water in the ITF region and cooler, denser, saline waters off Cape Leeuwin (Godfrey & Ridgway, 1985). The LC strength exhibits significant seasonal variability (Ridgway & Godfrey, 2015): At a cross section along 28°S, perpendicular to the West Australian coast, the mean annual transport amounts to 2.9 Sv but this value increases to more than 8 Sv in June (Wijeratne et al., 2018). A combination of two seasonal factors is responsible for the enhancement of the LC in austral autumn and winter: the fading of the opposing wind stress and a further increase in the steric height gradient along the pathway of the LC (Feng et al., 2003; Godfrey & Ridgway, 1985; Ridgway & Godfrey, 2015).

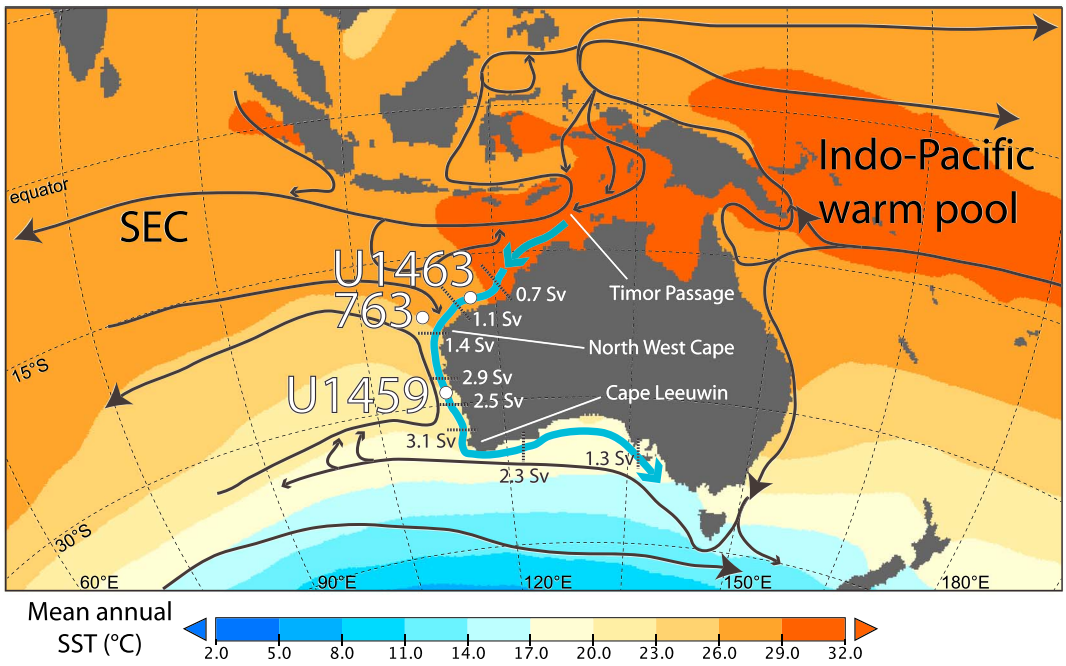

Figure 1. Site localities, major currents, and present-day (1971–2000) mean annual sea surface temperature (SST; Reynolds et al., 2002) in the Indo-Pacific region. The LC is indicated in blue. Surface transport across cross sections along the LC path are given in sverdrups (data from Wijeratne et al., 2018). LC = Leeuwin Current. SEC = South Equatorial Current.

The modern oceanography of the "unusual" LC is well studied but the pre-Quaternary history of this current remains contentious. The onset of "LC-style" circulation around Australia has been suggested as early as the Late Eocene (Diester-Haass & Zahn, 2001; McGowran et al., 1997). This timing corresponds to the beginning of a long-lasting tectonic evolution in the area, whereby the northward movement of Australia leads to a widening of the Tasman Street and a gradual restriction and reorganization of the ITF (Wyrwoll et al., 2009). By the time of the Pliocene, the paleogeographic setting of the Indo-Pacific was comparable to today, albeit with a smaller area above sea level within the throughflow region (Molnar & Cronin, 2015). From the Pliocene onward, ITF connectivity is a function of two distinct mechanisms: eustasy-driven ITF restriction through the emergence of shelf areas during sea level low stands (De Vleeschouwer et al., 2018; Di Nezio et al., 2016; Holbourn et al., 2011; Xu et al., 2006; Xu et al., 2008) and tectonic reorganization of the ITF network (Cane & Molnar, 2001; Christensen et al., 2017; Karas et al., 2009; Karas et al., 2011b; Karas et al., 2017; Molnar & Cronin, 2015).

International Ocean Discovery Program Expedition 356 Gallagher, Fulthorpe, Bogus, and the Expedition 356 Scientists (2017) obtained sediment cores along the LC pathway: on the northwest Australian shelf (Site U1463) and in the Perth Basin (Site U1459; Figure 1). The cored transect provides a Miocene-to-recent history of ITF, LC, and Australian climate evolution (Auer et al., 2019; Christensen et al., 2017; De Vleeschouwer et al., 2018; Groeneveld et al., 2017; Ishiwa et al., 2019) and complement sediments from previous drilling initiatives that have been employed to chart ITF variability (Karas et al., 2009, 2011a, 2011b, 2017). Based on Site U1463, Christensen et al. (2017) identified a major reorganization of Indian Ocean circulation around 3.3 Ma. Subsequently, De Vleeschouwer et al. (2018) used U1463 to detail a significant contraction of the LC at exactly that time and Auer et al. (2019) demonstrated the connection with the Sahul-Indian Ocean Bjerknes mechanism (Bjerknes, 1969; Di Nezio et al., 2016). However, the Pliocene variability of the LC south of the North West Cape remains undocumented to date and the effect of ITF variability on Indian Ocean circulation remains debated. Some authors suggest it as a major factor (Karas et al., 2017), while others find little influence (Petrick et al., 2015). To close this gap, we present multiproxy records from Site U1459 (Figure 1) detailing oceanographic conditions in the Perth Basin throughout the Pliocene. The U1459 Pliocene sedimentary archive documents LC variability at 28°S and allows for the assessment of consequences for ocean and climate.

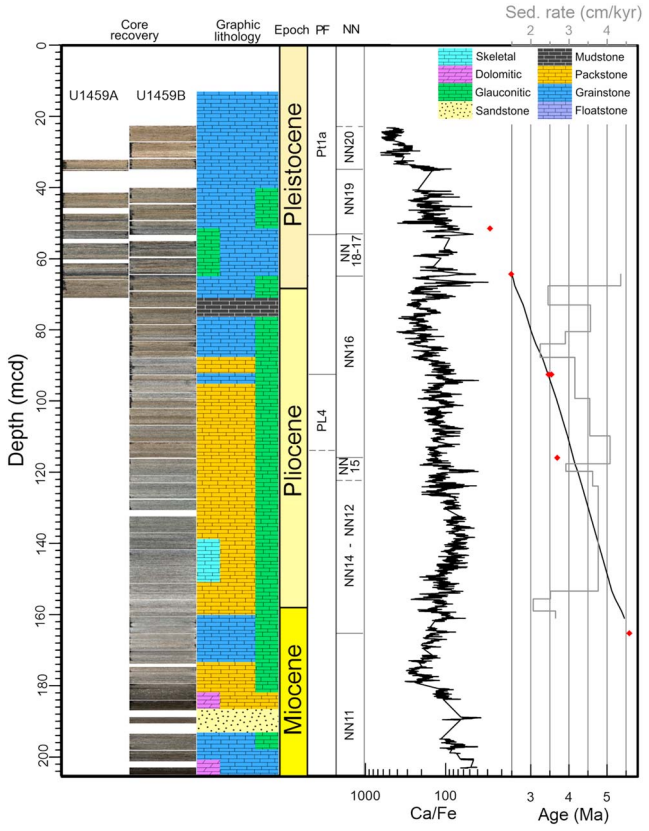

Figure 2. The U1459 lower Pliocene consists of unlithified light gray packstone with euhedral dolomite crystals. From 140 mcd upward, the sediment's color changes to light brown, dolomite content decreases, and glauconite content increases. Toward the uppermost Pliocene, glauconite becomes discernible macroscopically and occurs as scattered lenses and as glauconite-rich intervals. We refined the shipboard biostratigraphic age model (red diamonds) through astronomically tuning the Ca/Fe record (Figure S1). PF = planktonic foraminifer; NN = calcareous nannofossil; sed. rate = sedimentation rate; mcd = meter composite depth.

2. Materials and Methods

2.1. Site Description and Geochronology

Site U1459 was drilled at a present-day water depth of 192 m on the outer shelf, offshore the Houtman-Abrolhos reef complex. The modern-day LC system thus dictates characteristics of the overlying water column. During the Pliocene, Site U1459 was located at slightly greater water depth, on the outer shelf to upper slope. This is deduced from planktic/benthic foraminifera ratios, as well as from the somewhat steeper layering of Pliocene strata on the seismic profile across Site U1459 (see Table T10 and Figure F3 in Gallagher, Fulthorpe, Bogus, Auer, et al., 2017).

Two holes yield Pliocene sediments (Figure 2). A shipboard correlation between both holes was made using color reflectance data, resulting in composite depth scale (mcd) in which U1459A cores are shifted to fit with U1459B (Gallagher, Fulthorpe, Bogus, Auer, et al., 2017). A shipboard splice for Site U1459 was not constructed. Instead, we filled up stratigraphic gaps in U1459B with core sections from U1459A, where possible.

The X-ray fluorescence (XRF)-derived Ca/Fe shows an overall increase throughout the Pliocene. Superimposed on the long-term trend, significant meter-scale variability in Ca/Fe reflects fluctuations in carbonate content. We use the changes in Ca/Fe, in combination with geochronologic constraints from shipboard biostratigraphy (Gallagher, Fulthorpe, Bogus, Auer, et al., 2017), for astronomically tuning the U1459 stratigraphic column to the LR04 benthic oxygen isotope stack (Lisiecki & Raymo, 2005) and a southern hemisphere eccentricity-tilt-precession composite (Laskar et al., 2004; Figures 2 and S1 in the supporting information). Carbonate-rich intervals generally correspond to low TEX_{86} temperatures, more positive $\delta^{18}O_{G.sacculifer}$ values and lower K/Al. These relationships become particularly clear during the glacial events, indicated by gray bands on Figures 3 and S1. We associated the carbonate-rich intervals with cool intervals of the LR04 stack and minima in the eccentricity-tilt-precession composite. The tuning was constrained by six biostratigraphic datums, five from calcareous nannofossil, and one from planktonic foraminifera (see Table T8 in Gallagher, Fulthorpe, Bogus, Auer, et al., 2017) and consists of 15 age-depth tie points between 64 and 161 mcd, or 2.51 and 5.46 Ma (Table S1 and Figure S1). The shipboard *Reticulofenestra pseudoumbilicus* datum at 115.87 mcd (3.7 Ma in Gradstein et al., 2012] falls off the orbitally tuned age model (Figure 2). Yet, we deem our age model in this interval trustworthy because *R. pseudoumbilicus* is a last occurrence datum that indicates a minimum age. This datum was moreover assigned an older age of 3.82 Ma by Backman et al. (2012), reducing the discrepancy with our age model. Third, the orbital tuning between 100 and 125 mcd is robust with seven well-expressed 100-kyr eccentricity cycles between 3.7 and 4.4 Ma in the astronomical solution as well as in the Ca/Fe data (Figure S1).

Our age-depth model indicates highest sedimentation rates, around 4 cm/kyr, where $CaCO_3$ content is lowest, in the lower Pliocene. Therefore, we interpret the Ca/Fe fluctuations as dilution cycles, forming in response to recurring variations in clastic supply (Figure 2). Elemental Fe moreover shows strong covariation with Ti and Si (Figure S2), supporting the interpretation of those elements as tracers of detrital material.

2.2. Oxygen and Carbon Stable Isotope Analyses

A total of 143 stable carbon ($\delta^{13}C$) and oxygen ($\delta^{18}O$) isotope measurements were made on calcite tests of the shallow dwelling planktonic foraminifer *Globigerinoides sacculifer* (without sac-like chamber). In the framework of this study, we sampled the stratigraphic interval between 83.4 and 106.41 mcd from Hole U1459B at a median spatial resolution of 15 cm. Specimens were picked from the 315–355-μm-size fraction to avoid size effects in $\delta^{18}O$ values (Elderfield et al., 2002) and to be methodologically consistent with the nearby $\delta^{18}O_{G.}$

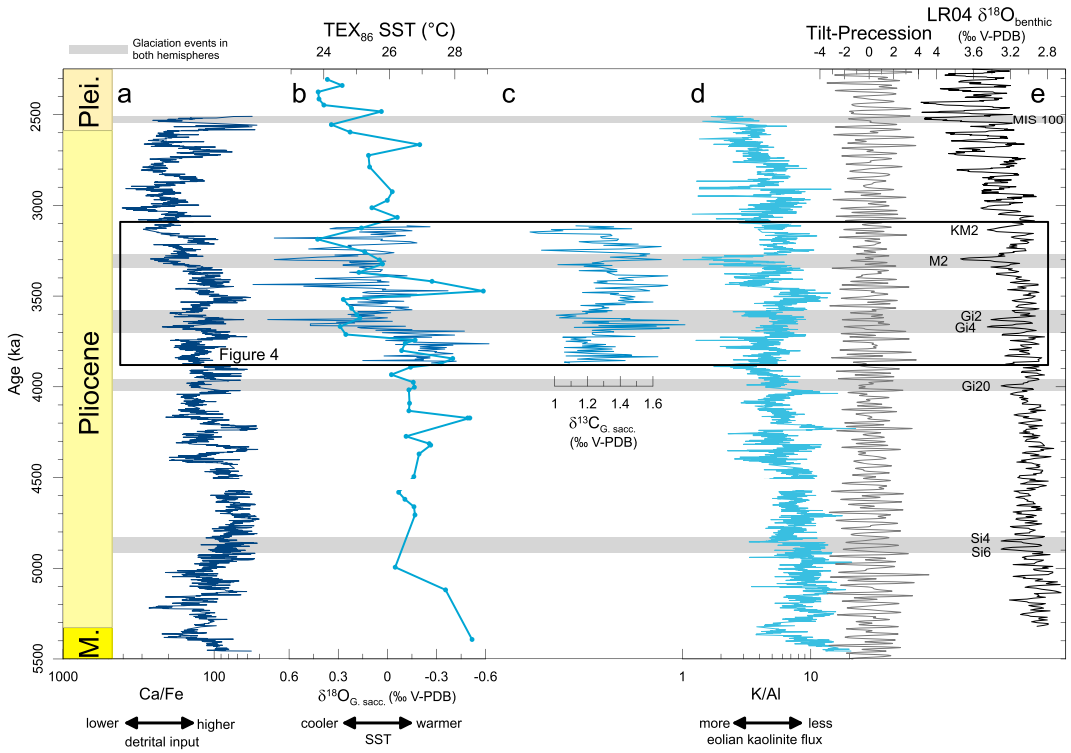

Figure 3. U1459 proxy time series. (a) XRF-derived Ca/Fe, proxy for detrital input. (b) Low-resolution TEX_{86} and high-resolution $\delta^{18}O_{G.sacculifer}$ reflect sea surface temperature (SST) evolution at different timescales. (c) $\delta^{13}C_{G.sacculifer}$ time series. (d) XRF-derived K/Al time series compared to a tilt-precession composite (Laskar et al., 2004). (e) LR04 stack indicates the global climate state. Horizontal gray bands highlight globally recognized glacials at 4.9, 4.0, 3.7-3.6, and 3.3 Ma (De Schepper et al., 2014) and 2.53 Ma (marine isotope stage 100). XRF = X-ray fluorescence.

sacculifer record for ODP Site 763A and International Ocean Discovery Program Site U1463 (De Vleeschouwer et al., 2018; Karas et al., 2011b). All samples were measured on a Finnigan MAT 251 gas isotope ratio mass spectrometer connected to a Kiel III automated carbonate preparation device at the Center for Marine Environmental Sciences (MARUM). Data are reported in standard delta-notation versus V-PDB. We calibrated all measurements against the in-house standard (ground Solnhofen limestone), which in turn is calibrated against the NBS-19 reference. Over the measurement period the standard deviations of the in-house standard ($N = 41$) were 0.04‰ for $\delta^{13}C$ and 0.06‰ for $\delta^{18}O$.

2.3. TEX_{86} Paleothermometry

TEX_{86} analyses were carried out in Max-Planck-Institute for Chemistry. Lipids were extracted from the sediment samples using a Dionex accelerated solvent extractor (ASE 350). The extraction was performed using a method of simultaneous extraction and chromatographic separation of different fractions by polarity during the extraction process. After the extraction, the samples were dried using a roto-evaporative system. The polar fraction was then analyzed using high-performance liquid chromatography mass spectrometry following the methods described by Hopmans et al. (2004). The TEX_{86} sea surface temperature (SST) data set was subjected to a number of tests to check the marine origin of the glycerol dialkyl glycerol tetraethers (GDGTs), as well as other potential nonthermal influences in the reconstructed SST. We estimated the GDGT-0% (Weijers et al., 2006), methane index (Zhang et al., 2014), $\%GDGT_{RS}$ (Inglis et al., 2015), branched and isoprenoid tetraether (Schouten et al., 2013; Weijers et al., 2006), and ring index (Zhang et al., 2016). All samples were within the recommended values for reliable paleo-SST reconstructions. SST estimates were obtained from the TEX_{86} values using the BAYSPAR calibration (Tierney & Tingley, 2014). The 5th and 95th percentiles of the BAYSPAR calibration are plotted in Figure S3. Based on the observation of the variability of the in-house standard within this batch, the analytical precision for TEX86 is ±0.4 °C (2σ).

2.4. XRF Core Scanning

The elemental composition of U1459 sediments was measured on the archive-half core surfaces using the third-generation Avaatech XRF core scanner at the XRF Core Scanning Facility of the Gulf Coast Repository at Texas A&M University in July 2016. Measurements were taken at a spatial resolution of 3 cm, at source energies of 9 kV (no filter, 0.25 mA) and 30 kV (Pd filter, 1.25 mA) and a 6-s count time for each measurement at each energy. Where possible, stratigraphic gaps in the recovery in Hole U1459B were closed with sections from Hole U1459A (Figure 2). Element intensities were obtained by processing raw X-ray spectra using the iterative least square software (WIN AXIL) package from Canberra Eurisys.

3. Reconstructing the Pliocene Climate of southwest Australia

The low-resolution TEX_{86} SST reconstruction for Site U1459 suggests temperatures between 23.8 and 28.9 °C throughout the Pliocene. The lowest Pliocene TEX_{86} temperature occurs during marine isotope stage (MIS) KM2, at 3.13 Ma, one of the cool spells during the mid-Pliocene warm period. This lowest temperature (23.8 °C) is however still warmer than today's mean annual SST at Site U1459 of about 22.8 °C (Reynolds et al., 2002). The Pliocene Model Intercomparison project suggests SSTs in the Perth basin to be 1–3° warmer during the Pliocene compared to the preindustrial (Figure 1 in Dowsett et al., 2013 [405 ppm CO_2]; Figure 2c in Haywood et al., 2013 [405 ppm CO_2]; Figure 9 in Hunter et al., 2019 [450, 400, 350, and 280 ppm CO_2]). We report temperatures up to 6 °C warmer than the present day, particularly for the early Pliocene. We ascribe this additional amplitude to long-term changes in the boundary conditions (paleogeography, gateways, and atmospheric chemistry) and short-term changes in orbital forcing that were not considered in the climate simulations. The high-resolution $\delta^{18}O_{G.sacculifer}$ record exhibits covariation with the low-resolution TEX_{86} temperatures (Figures 3b and S4), suggesting minimal contribution from global and/or local changes in the $\delta^{18}O$ of seawater $\delta^{18}O_{sw}$) to the measured $\delta^{18}O$ of calcite. The total $\delta^{18}O_{G.sacculifer}$ range amounts to 1.2‰, which translates to ~6 °C temperature amplitude, regardless of whether we use a constant $\delta^{18}O_{sw}$, or the Pliocene global $\delta^{18}O_{sw}$ reconstruction of Rohling et al. (2014); Figure S5, if the effects of salinity change are considered negligible. The $\delta^{18}O_{G.sacculifer}$ amplitude is thus of the same order of magnitude as TEX_{86} temperature variability. Despite the large uncertainty on the BAYSPAR TEX_{86} calibration and the fact that Pliocene $\delta^{18}O_{sw}$ is unknown, the consistency between the two temperature proxies suggests that SSTs in the Perth basin were significantly warmer than today throughout the entire Pliocene. This would imply that the LC was active during the entire epoch. Nevertheless, both proxies indicate significant SST variability, up to 5 °C, hinting toward Pliocene LC variability. This variability is discussed further in the manuscript.

The K/Al proxy provides insight in hydroclimate changes throughout the Pliocene in the hinterland. Minima in K/Al indicate periods with an increased kaolinite share in the clay mineral assemblage at Site U1459. In the marine basins surrounding southwest Australia, kaolinite is sourced from the deeply weathered, kaolinite-rich, lateritic residuum of the Yilgarn Craton (Anand, 2001). This kaolinite is primarily transported through wind erosion when the vegetation cover is reduced (Mallinson et al., 2003). For the Pleistocene, the collapse of forest vegetation in southwest Australia happens under glacial conditions (Sniderman et al., 2019, and references therein) and the covariation between $\delta^{18}O$ and K/Al in our data set suggests that this phase relationship remained constant over the Plio-Pleistocene (Figure S6). Under warm and wet conditions, to the contrary, the vegetation cover would increase, the eolian flux of kaolinite to the Perth basin would decrease, but the fluvial transport of clays would significantly increase. This climate mechanism fits the U1459 XRF records, as maxima in K/Al (low kaolinite in clay assemblage) correspond to minima in Ca/Fe (high detrital input).

We observe a long-term decrease in K/Al over the course of the Pliocene, suggesting a progressive drying of the climate in southwest Australia, which continues into the Pleistocene. In fact, Groeneveld et al. (2017) showed that the hydroclimate of southwest Australia was perennially wet in the Late Miocene (8 Ma), as it was under the direct influence of the Westerlies. Since 8 Ma, the latitudinal position of the Westerlies remained more or less stable, but Australia traveled northward tectonically with ~70 km/Myr. This gradually moved southwest Australia out of the ever-wet Westerlies into a more Mediterranean-style climate with seasonal aridity. The long-term Pliocene decrease in K/Al at U1459 is thus the expression of this long-term regional climate development. This interpretation is also in agreement with an upper Pliocene lake sequence

in southwestern Australia, suggesting a warm and seasonally wet climate between 3.6 and 2.5 Ma (Dodson & Macphail, 2004; Dodson & Ramrath, 2001).

Superimposed on the long-term decreasing K/Al trend, clear astronomically paced variations in K/Al show remarkable covariability with a tilt-precession (TP) composite (Figure S7). Insolation regimes that are characterized by high seasonality (high TP values) correspond to less eolian kaolinite fluxes (high K/Al). The explanation for this pattern likely involves an intensification of winter precipitation under such an insolation regime. The potential nullification of summer precipitation does not have much influence, as the subtropical woodland, scrub and heath vegetation is resistant to amplified seasonal drought. Hence, we hypothesize that high-seasonality orbital configurations resulted in a denser vegetation cover and less eolian erosion. Low-seasonality configurations (low TP), on the other hand, likely had a negative impact on the amount of winter precipitation, and therefore annual precipitation. This more arid hydroclimate regime led to a reduced total detrital input at Site U1459 but to an increase in eolian flux, rich in kaolinite. We thus interpret carbonate-rich intervals to reflect dampened winter precipitation and, as explained above, we assume these intervals to correspond with Pliocene glacials in the LR04 stack. Moreover, this interpretation sheds new light on the work of Dodson and Macphail (Dodson & Macphail, 2004) who reported two "aridity events" in southwest Australia between ~2.6 and 2.5 Ma. At U1459, one of these events could find its expression in a distinct high-carbonate interval just above the Plio-Pleistocene boundary that corresponds to the MIS 100 glacial in our orbitally tuned age model.

4. Drivers of LC Variability

The Pliocene variability of the LC south of the Northwest Cape remains undocumented to date. Here, we compare the high-resolution $\delta^{18}O_{G.sacculifer}$ record of U1459 to its contemporaneous counterparts at Site 763 (Exmouth Plateau) and Site U1463 (Northwest Shelf) between 3.9 and 3.1 Ma. The latter two sites, both north of the Northwest Cape, have nearly identical isotopic signatures during the studied time slice (De Vleeschouwer et al., 2018). Their isotopic offset with U1459 ranges between 0.8‰ and 2‰ and is independent of global changes in ice volume, as the associated changes in the $\delta 18O_{sw}$ would affect all sites equally (Figures 4a and 4c). Therefore, relatively small isotopic offsets between the northern sites and Site U1459 are indicative of a strong LC, since a stronger current transports more hot water faster from the Northwest Shelf toward the Perth basin, flattening out the isotopic gradient. The U1459 versus Site 763 comparison (Figures 4a and 4b) exhibits a stepped increase in isotopic offset just prior to the global glaciation event at 3.7–3.6 Ma. This 0.6‰ increase marks a regime shift after which the LC never returns to its early Pliocene state. The TEX_{86} SST at Site U1459 exhibit a 2 °C temperature drop at the same time, also marking a permanent change toward cooler SSTs. A tectonic reorganization of the ITF is the likely cause of this abrupt shift, as the timing corresponds to the collision of the Banda volcanic arc with the Australian margin in Timor (Hall, 2009). We compare this step increase in $\Delta\delta^{18}O$ to a modeling results by Song et al. (Figure 4C in Song et al., 2007), despite some important differences in boundary conditions. These authors report a 1.5 °C cooling in the Perth Basin, but only a 0.5 °C cooling north of the Northwest Cape, after a complete closure of the ITF with respect to the present-day situation. The model predicts an equal increase in salinity at both sites in response to the closure. This comparison indicates that the observed 0.6‰ step increase and the 2 °C temperature drop are consistent with the expected response to a tectonic reorganization of the ITF region.

We assess LC variability in the subsequent period (3.7–3.1 Ma) through the comparison of Site U1459 and U1463. The isotopic offset between both sites is characterized by intriguing variability. Here, we postulate that a large part of this variability can be described by a combination of only two factors. The first factor (Figures 4d and 4e) is the 21 June interhemisphere insolation gradient (SITIG, 23°N to 23°S; Bosmans et al., 2015; Reichart, 1997). When the interhemisphere gradient is large during austral winter, the Hadley cell above Australia is strengthened (Bosmans et al., 2015). As a consequence, the southeasterly winds blowing off the Australian continent during winter are intensified (Bosmans et al., 2015), leading to LC favorable wind stress and Ekman transport. Moreover, the SITIG series in Figure 4e resembles the time series of the length of the austral winter half year (Laskar et al., 2004). This means that during maxima in SITIG, the duration of the season of maximum LC strength is prolonged. The second factor (Figures 4d and 4f) is sea level as a modulator of ITF connectivity. Weaker ITF connectivity during sea level lowstands leads to a

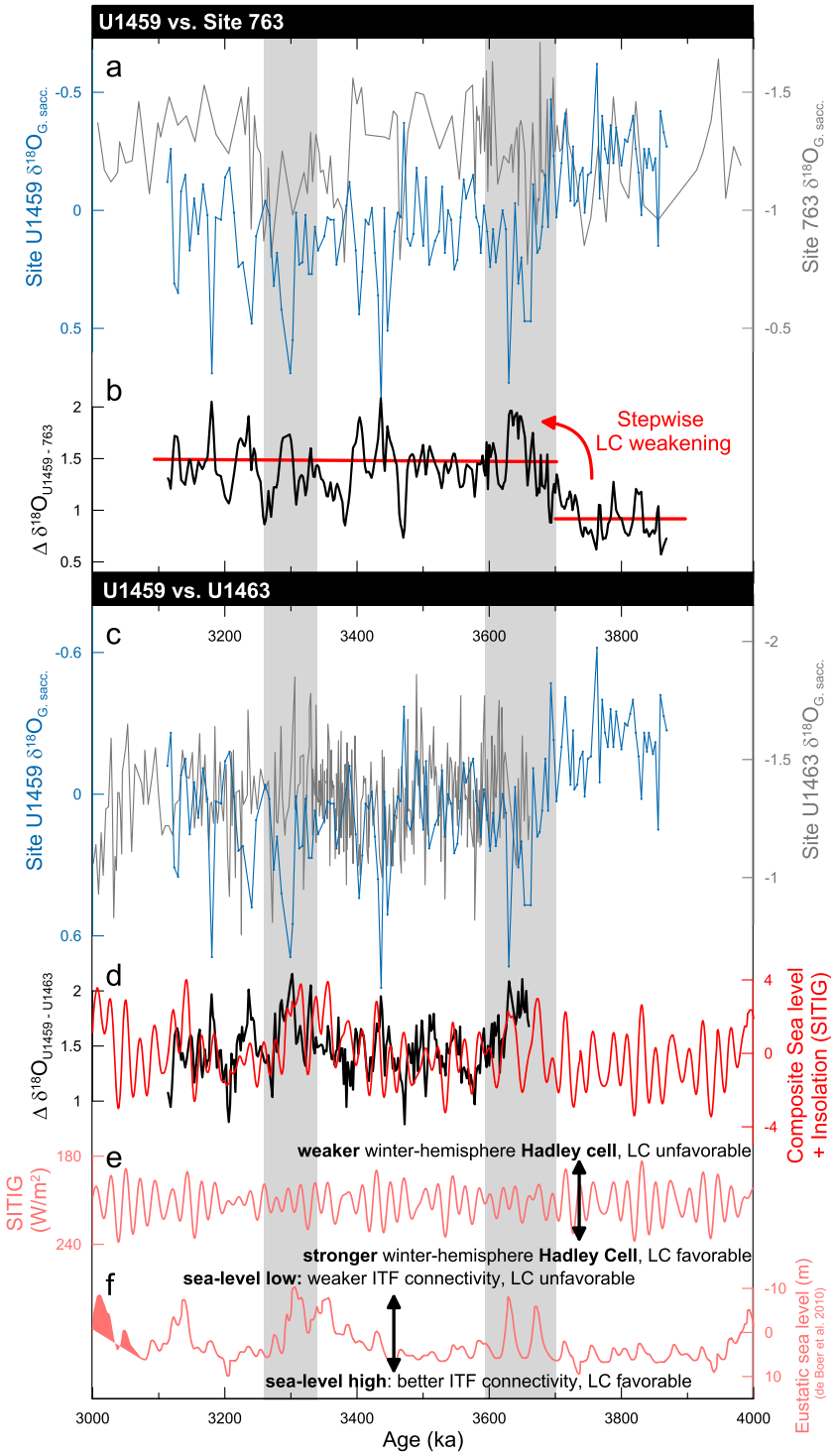

Figure 4. Isotopic gradients along the Leeuwin Current (LC) pathway. (a, b) Comparison of $\delta^{18}O_{G.sacculifer}$ between Site 763 (Exmouth Plateau; Karas et al., 2011b) and Site U1459. (c, d) Comparison of the $\delta^{18}O_{G.\ sacculifer}$ between Site U1463 (Northwest Shelf; De Vleeschouwer et al., 2018) and Site U1459. The gradient between both sites resembles a combination of (e) 21 June interhemisphere insolation gradient (SITIG; Reichart, 1997) and (f) eustatic sea level (de Boer et al., 2010). Gray bands highlight globally recognized glacials at 3.7–3.6 and 3.3 Ma (De Schepper et al., 2014). ITF = Indonesian Throughflow.

reduction in source waters for the LC. As a result, the current will be weakened and the reduction in overspill of warm equatorial water from the Pacific into the Indian Ocean will propagate along the LC pathway (Schneider, 1998; Song et al., 2007). This mechanism operates in response to relative sea level changes in the archipelago, as already became clear with the stepwise LC weakening around 3.7 Ma. However, we approach this mechanism through the eustatic sea level reconstruction of de Boer et al. (2010); Figures 4d and 4f), as relevant relative sea level reconstructions are not available. We opted for the de Boer et al. (2010) reconstruction because it has conservative low sea level variability except for the globally recognized glaciation events. Indeed, the globally recognized glaciation events at 3.3 (MIS M2) and 3.7–3.6 Ma are marked maxima of the $\Delta\delta^{18}O_{U1463\text{-}U1459}$. At 3.3 Ma, the isotopic gradient between both sites amounts 2.01‰, which is twice as much as the equivalent value 100 kyr earlier. This change in gradient implies that the latitudinal SST gradient doubled its steepness during MIS M2, compared to the preceding interglacial. These results highlight the importance of Pliocene global sea level lows on Southern Hemisphere ocean circulation. A secondary maximum in $\Delta\delta^{18}O_{U1463\text{-}U1459}$ occurs at 3.43 Ma, when a minor sea level low and a SITIG minimum reinforce each other to force a LC intensity minimum.

5. Conclusions

The LC transported warm waters into the Perth basin throughout the entire Pliocene but experienced significant variability in its intensity. We disentangled Pliocene LC variability in three main drivers: tectonic reorganizations, sea level variability on orbital timescales, and direct orbital forcing of wind patterns that hampered or promoted the LC. The first two drivers are directly linked to the connectivity between the Pacific and Indian Oceans through the Indonesian gateway. This study thus shows that ITF connectivity influences Indian Ocean circulation, also outside its immediate outflow region.

Acknowledgments
This research used samples and data provided by the International Ocean Discovery Program (IODP). We thank all IODP Expedition 356 scientific participants and crew for making this study possible. The VOCATIO Foundation provided funding through a scholarship to D. D. V. (2016 promotion). At the time of writing, D. D. V. was a postdoctoral researcher in ERC Consolidator grant "EARTHSEQUENCING" (Grant 617462) and is currently funded through the Cluster of Excellence "The Ocean Floor - Earth's Uncharted Interface". The Max Plank Society provided funding through a postdoctoral grant to B. P. We want to explicitly thank Heiko Pälike, Gerald Haug, Kara Bogus, Lars Reuning, and Gerald Auer for scientific discussions and practical support. We are grateful to Cecilia McHugh and one anonymous reviewer for their thorough evaluation of this work. All proxy data used in this manuscript are available at https://doi.pangaea.de/10.1594/PANGAEA.903102 (U1459), https://doi.pangaea.de/10.1594/PANGAEA.892422 (U1463), and ftp://ftp.ncdc.noaa.gov/pub/data/paleo/contributions_by_author/karas2011/karas2011.txt (Site 763).

References

Anand, R. (2001). Evolution, classification and use of ferruginous regolith materials in gold exploration, Yilgarn Craton, Western Australia. *Geochemistry: Exploration, Environment, Analysis*, *1*, 221–236.

Auer, G., De Vleeschouwer, D., Smith, R. A., Bogus, K., Groeneveld, J., Grunert, P., et al. (2019). Timing and pacing of Indonesian Throughflow restriction and its connection to Late Pliocene climate shifts. *Paleoceanography and Paleoclimatology*, *34*, 635–657. https://doi.org/10.1029/2018PA003512

Backman, J., Raffi, I., Rio, D., Fornaciari, E., & Pälike, H. (2012). Biozonation and biochronology of Miocene through Pleistocene calcareous nannofossils from low and middle latitudes. *Newsletters on Stratigraphy*, *45*(3), 221–244. https://doi.org/10.1127/0078-0421/2012/0022

Bjerknes, J. (1969). Atmospheric teleconnections from the equatorial Pacific. *Monthly Weather Review*, *97*(3), 163–172. https://doi.org/10.1175/1520-0493(1969)097<0163:Atftep>2.3.Co;2

Bosmans, J. H. C., Hilgen, F. J., Tuenter, E., & Lourens, L. J. (2015). Obliquity forcing of low-latitude climate. *Climate of the Past*, *11*(10), 1335–1346. https://doi.org/10.5194/cp-11-1335-2015

Cane, M. A., & Molnar, P. (2001). Closing of the Indonesian seaway as a precursor to east African aridification around 3–4 million years ago. *Nature*, *411*(6834), 157–162. https://doi.org/10.1038/35075500

Christensen, B. A., Renema, W., Henderiks, J., De Vleeschouwer, D., Groeneveld, J., Castañeda, I. S., et al., & IODP Expedition 356 Scientists (2017). Indonesian Throughflow drove Australian climate from humid Pliocene to arid Pleistocene. *Geophysical Research Letters*, *44*, 6914–6925. https://doi.org/10.1002/2017GL072977

de Boer, B., van de Wal, R. S. W., Bintanja, R., Lourens, L. J., & Tuenter, E. (2010). Cenozoic global ice-volume and temperature simulations with 1-D ice-sheet models forced by benthic δ18O records. *Annals of Glaciology*, *51*(55), 23–33. https://doi.org/10.3189/172756410791392736

De Schepper, S., Gibbard, P. L., Salzmann, U., & Ehlers, J. (2014). A global synthesis of the marine and terrestrial evidence for glaciation during the Pliocene Epoch. *Earth-Science Reviews*, *135*, 83–102. https://doi.org/10.1016/j.earscirev.2014.04.003

De Vleeschouwer, D., Auer, G., Smith, R., Bogus, K., Christensen, B., Groeneveld, J., et al. (2018). The amplifying effect of Indonesian Throughflow heat transport on Late Pliocene Southern Hemisphere climate cooling. *Earth and Planetary Science Letters*, *500*, 15–27. https://doi.org/10.1016/j.epsl.2018.07.035

Di Nezio, P. N., Timmermann, A., Tierney, J. E., Jin, F.-F., Otto-Bliesner, B., Rosenbloom, N., et al. (2016). The climate response of the Indo-Pacific warm pool to glacial sea level. *Paleoceanography*, *31*, 866–894. https://doi.org/10.1002/2015PA002890

Diester-Haass, L., & Zahn, R. (2001). Paleoproductivity increase at the Eocene–Oligocene climatic transition: ODP/DSDP sites 763 and 592. *Palaeogeography, Palaeoclimatology, Palaeoecology*, *172*(1-2), 153–170. https://doi.org/10.1016/S0031-0182(01)00280-2

Dodson, J. R., & Macphail, M. K. (2004). Palynological evidence for aridity events and vegetation change during the Middle Pliocene, a warm period in Southwestern Australia. *Global and Planetary Change*, *41*(3-4), 285–307. https://doi.org/10.1016/j.gloplacha.2004.01.013

Dodson, J. R., & Ramrath, A. (2001). An Upper Pliocene lacustrine environmental record from south-Western Australia—Preliminary results. *Palaeogeography, Palaeoclimatology, Palaeoecology*, *167*(3-4), 309–320. https://doi.org/10.1016/S0031-0182(00)00244-3

Dowsett, H. J., Foley, K. M., Stoll, D. K., Chandler, M. A., Sohl, L. E., Bentsen, M., et al. (2013). Sea surface temperature of the mid-Piacenzian ocean: A data-model comparison. *Scientific Reports*, *3*(1). https://doi.org/10.1038/srep02013, https://www.nature.com/articles/srep02013#supplementary-information

Elderfield, H., Vautravers, M., & Cooper, M. (2002). The relationship between shell size and Mg/Ca, Sr/Ca, δ18O, and δ13C of species of planktonic foraminifera. *Geochemistry, Geophysics, Geosystems*, *3*(8), 1052. https://doi.org/10.1029/2001GC000194

Feng, M., Majewski, L. J., Fandry, C. B., & Waite, A. M. (2007). Characteristics of two counter-rotating eddies in the Leeuwin Current system off the Western Australian coast. *Deep Sea Research Part II: Topical Studies in Oceanography*, *54*(8-10), 961–980. https://doi.org/10.1016/j.dsr2.2006.11.022

Feng, M., Meyers, G., Pearce, A., & Wijffels, S. (2003). Annual and interannual variations of the Leeuwin Current at 32°S. *Journal of Geophysical Research*, *108*(C11), 3355. https://doi.org/10.1029/2002JC001763

Furue, R., Guerreiro, K., Phillips, H. E., Julian, P., McCreary, J., & Bindoff, N. L. (2017). On the Leeuwin Current System and its linkage to zonal flows in the south Indian Ocean as inferred from a gridded hydrography. *Journal of Physical Oceanography*, *47*(3), 583–602. https://doi.org/10.1175/jpo-d-16-0170.1

Gallagher, S. J., Fulthorpe, C. S., Bogus, K., Auer, G., Baranwal, S., Castañeda, I. S., et al. (2017). Site U1459. In S. J. Gallagher, C. S. Fulthorpe, K. Bogus, & the Expedition 356 Scientists (Eds.), *Indonesian Throughflow* (Vol. 356, Chap. 4, pp. 1–41). College Station, TX: Proceedings of the International Ocean Discovery Program. https://doi.org/10.14379/iodp.proc.356.104.2017

Gallagher, S. J., Fulthorpe, C. S., Bogus, K., & the Expedition 356 Scientists (2017). *Indonesian Throughflow*, (Vol. 356). College Station, TX: International Ocean Discovery Program. https://doi.org/10.14379/iodp.proc.356.2017

Godfrey, J., & Ridgway, K. (1985). The large-scale environment of the poleward-flowing Leeuwin Current, Western Australia: longshore steric height gradients, wind stresses and geostrophic flow. *Journal of Physical Oceanography*, *15*(5), 481–495. https://doi.org/10.1175/1520-0485(1985)015<0481:TLSEOT>2.0.CO;2

Gradstein, F. M., Ogg, J. G., Schmitz, M., & Ogg, G. (2012). *The geologic time scale 2012 2-volume set*. Oxford, UK: Elsevier.

Groeneveld, J., Henderiks, J., Renema, W., McHugh, C. M., De Vleeschouwer, D., Christensen, B. A., et al., & Expedition 356 Scientists (2017). Australian shelf sediments reveal shifts in Miocene Southern Hemisphere westerlies. *Science Advances*, *3*(5), e1602567. https://doi.org/10.1126/sciadv.1602567

Hall, R. (2009). Southeast Asia's changing palaeogeography. *Blumea*, *54*(1), 148–161. https://doi.org/10.3767/000651909X475941

Haywood, A. M., Hill, D. J., Dolan, A. M., Otto-Bliesner, B. L., Bragg, F., Chan, W. L., et al. (2013). Large-scale features of Pliocene climate: Results from the Pliocene Model Intercomparison Project. *Climate of the Past*, *9*(1), 191–209. https://doi.org/10.5194/cp-9-191-2013

Holbourn, A., Kuhnt, W., & Xu, J. (2011). Indonesian Throughflow variability during the last 140 ka: The Timor Sea outflow. *Geological Society, London, Special Publications*, *355*(1), 283–303. https://doi.org/10.1144/sp355.14

Holloway, P. E. (1995). Leeuwin current observations on the Australian North West Shelf, May–June 1993. *Deep Sea Research Part I: Oceanographic Research Papers*, *42*(3), 285–305. https://doi.org/10.1016/0967-0637(95)00004-P

Hopmans, E. C., Weijers, J. W. H., Schefuß, E., Herfort, L., Sinninghe Damsté, J. S., & Schouten, S. (2004). A novel proxy for terrestrial organic matter in sediments based on branched and isoprenoid tetraether lipids. *Earth and Planetary Science Letters*, *224*(1-2), 107–116. https://doi.org/10.1016/j.epsl.2004.05.012

Hunter, S. J., Haywood, A. M., Dolan, A. M., & Tindall, J. C. (2019). The HadCM3 contribution to PlioMIP Phase 2 Part 1: Core and Tier 1 experiments. *Climate of the Past Discussions*, *2019*, 1–38. https://doi.org/10.5194/cp-2018-180

Inglis, G. N., Farnsworth, A., Lunt, D., Foster, G. L., Hollis, C. J., Pagani, M., et al. (2015). Descent toward the Icehouse: Eocene sea surface cooling inferred from GDGT distributions. *Paleoceanography*, *30*, 1000–1020. https://doi.org/10.1002/2014pa002723

Ishiwa, T., Yokoyama, Y., Reuning, L., McHugh, C. M., De Vleeschouwer, D., & Gallagher, S. J. (2019). Australian Summer Monsoon variability in the past 14,000 years revealed by IODP Expedition 356 sediments. *Progress in Earth and Planetary Science*, *6*(1), 17. https://doi.org/10.1186/s40645-019-0262-5

Karas, C., Nürnberg, D., Bahr, A., Groeneveld, J., Herrle, J. O., Tiedemann, R., & deMenocal, P. B. (2017). Pliocene oceanic seaways and global climate. *Scientific Reports*, *7*(1), 1–8. https://doi.org/10.1038/srep39842

Karas, C., Nürnberg, D., Gupta, A. K., Tiedemann, R., Mohan, K., & Bickert, T. (2009). Mid-Pliocene climate change amplified by a switch in Indonesian subsurface throughflow. *Nature Geoscience*, *2*(6), 434–438. https://doi.org/10.1038/ngeo520

Karas, C., Nürnberg, D., Tiedemann, R., & Garbe-Schonberg, D. (2011a). Pliocene climate change of the Southwest Pacific and the impact of ocean gateways. *Earth and Planetary Science Letters*, *301*(1-2), 117–124. https://doi.org/10.1016/j.epsl.2010.10.028

Karas, C., Nürnberg, D., Tiedemann, R., & Garbe-Schonberg, D. (2011b). Pliocene Indonesian Throughflow and Leeuwin Current dynamics: Implications for Indian Ocean polar heat flux. *Paleoceanography*, *26*, PA2217. https://doi.org/10.1029/2010pa001949

Laskar, J., Robutel, P., Joutel, F., Gastineau, M., Correia, A., & Levrard, B. (2004). A long-term numerical solution for the insolation quantities of the Earth. *Astronomy & Astrophysics*, *428*(1), 261–285. https://doi.org/10.1051/0004-6361:20041335

Lisiecki, L. E., & Raymo, M. E. (2005). A Pliocene-Pleistocene stack of 57 globally distributed benthic δ18O records. *Paleoceanography*, *20*, PA1003. https://doi.org/10.1029/2004PA001071

Mallinson, D. J., Flower, B., Hine, A., Brooks, G., & Garza, R. M. (2003). Paleoclimate implications of high latitude precession-scale mineralogic fluctuations during early Oligocene Antarctic glaciation: the Great Australian Bight record. *Global and Planetary Change*, *39*(3-4), 257–269. https://doi.org/10.1016/S0921-8181(03)00119-X

McGowran, B., Li, Q., Cann, J., Padley, D., McKirdy, D. M., & Shafik, S. (1997). Biogeographic impact of the Leeuwin Current in southern Australia since the late middle Eocene. *Palaeogeography, Palaeoclimatology, Palaeoecology*, *136*(1-4), 19–40. https://doi.org/10.1016/S0031-0182(97)00073-4

Molnar, P., & Cronin, T. W. (2015). Growth of the Maritime Continent and its possible contribution to recurring Ice Ages. *Paleoceanography*, *30*, 196–225. https://doi.org/10.1002/2014PA002752

Pearce, A. (1991). Eastern boundary currents of the southern hemisphere. *Journal of the Royal Society of Western Australia*, *74*, 35–45.

Petrick, B., McClymont, E. L., Felder, S., Rueda, G., Leng, M. J., & Rosell-Melé, A. (2015). Late Pliocene upwelling in the Southern Benguela region. *Palaeogeography, Palaeoclimatology, Palaeoecology*, *429*(Supplement C), 62–71. https://doi.org/10.1016/j.palaeo.2015.03.042

Reichart, G.-J. (1997). Late Quaternary variability of the Arabian Sea monsoon and oxygen minimum zone. Utrecht University, Utrecht.

Reynolds, R. W., Rayner, N. A., Smith, T. M., Stokes, D. C., & Wang, W. (2002). An Improved In Situ and Satellite SST Analysis for Climate. *Journal of Climate*, *15*(13), 1609–1625. https://doi.org/10.1175/1520-0442(2002)015<1609:Aiisas>2.0.Co;2

Ridgway, K. R., & Godfrey, J. S. (2015). The source of the Leeuwin Current seasonality. *Journal of Geophysical Research: Oceans*, *120*, 6843–6864. https://doi.org/10.1002/2015JC011049

Rohling, E. J., Foster, G. L., Grant, K. M., Marino, G., Roberts, A. P., Tamisiea, M. E., & Williams, F. (2014). Sea-level and deep-sea-temperature variability over the past 5.3 million years. *Nature*, *508*(7497), 477–482. https://doi.org/10.1038/nature13230

Schneider, N. (1998). The Indonesian Throughflow and the Global Climate System. *Journal of Climate*, *11*(4), 676–689. https://doi.org/10.1175/1520-0442(1998)011<0676:Titatg>2.0.Co;2

Schouten, S., Hopmans, E. C., & Sinninghe Damsté, J. S. (2013). The organic geochemistry of glycerol dialkyl glycerol tetraether lipids: A review. *Organic Geochemistry*, *54*, 19–61. https://doi.org/10.1016/j.orggeochem.2012.09.006

Smith, R. L., Huyer, A., Godfrey, J. S., & Church, J. A. (1991). The Leeuwin Current off Western Australia, 1986–1987. *Journal of Physical Oceanography*, *21*(2), 323–345. https://doi.org/10.1175/1520-0485(1991)021<0323:Tlcowa>2.0.Co;2

Sniderman, J. M. K., Hellstrom, J., Woodhead, J. D., Drysdale, R. N., Bajo, P., Archer, M., & Hatcher, L. (2019). Vegetation and climate change in Southwestern Australia during the Last Glacial Maximum. *Geophysical Research Letters*, *46*, 1709–1720. https://doi.org/10.1029/2018GL080832

Song, Q., Vecchi, G. A., & Rosati, A. J. (2007). The role of the Indonesian Throughflow in the Indo–Pacific climate variability in the GFDL coupled climate model. *Journal of Climate*, *20*(11), 2434–2451. https://doi.org/10.1175/jcli4133.1

Thompson, P. A., Wild-Allen, K., Lourey, M., Rousseaux, C., Waite, A. M., Feng, M., & Beckley, L. E. (2011). Nutrients in an oligotrophic boundary current: Evidence of a new role for the Leeuwin Current. *Progress in Oceanography*, *91*(4), 345–359. https://doi.org/10.1016/j.pocean.2011.02.011

Tierney, J. E., & Tingley, M. P. (2014). A Bayesian, spatially-varying calibration model for the TEX86 proxy. *Geochimica et Cosmochimica Acta*, *127*, 83–106. https://doi.org/10.1016/j.gca.2013.11.026

Waite, A. M., Thompson, P. A., Pesant, S., Feng, M., Beckley, L. E., Domingues, C. M., et al. (2007). The Leeuwin Current and its eddies: An introductory overview. *Deep Sea Research Part II: Topical Studies in Oceanography*, *54*(8-10), 789–796. https://doi.org/10.1016/j.dsr2.2006.12.008

Weaver, A. J., & Middleton, J. H. (1990). An analytic model for the Leeuwin Current off western Australia. *Continental Shelf Research*, *10*(2), 105–122. https://doi.org/10.1016/0278-4343(90)90025-H

Weijers, J. W. H., Schouten, S., Hopmans, E. C., Geenevasen, J. A. J., David, O. R. P., Coleman, J. M., et al. (2006). Membrane lipids of mesophilic anaerobic bacteria thriving in peats have typical archaeal traits. *Environmental Microbiology*, *8*(4), 648–657. https://doi.org/10.1111/j.1462-2920.2005.00941.x

Wijeratne, S., Pattiaratchi, C., & Proctor, R. (2018). Estimates of surface and subsurface boundary current transport around Australia. *Journal of Geophysical Research: Oceans*, *123*, 3444–3466. https://doi.org/10.1029/2017JC013221

Woo, M., & Pattiaratchi, C. (2008). Hydrography and water masses off the western Australian coast. *Deep Sea Research Part I: Oceanographic Research Papers*, *55*(9), 1090–1104. https://doi.org/10.1016/j.dsr.2008.05.005

Wyrwoll, K.-H., Greenstein, B. J., & Kendrick, G. (2009). The palaeoceanography of the Leeuwin Current: implications for a future world. *Journal of the Royal Society of Western Australia*, *92*(2), 37–51.

Xu, J., Holbourn, A., Kuhnt, W., Jian, Z., & Kawamura, H. (2008). Changes in the thermocline structure of the Indonesian outflow during Terminations I and II. *Earth and Planetary Science Letters*, *273*(1-2), 152–162. https://doi.org/10.1016/j.epsl.2008.06.029

Xu, J., Kuhnt, W., Holbourn, A., Andersen, N., & Bartoli, G. (2006). Changes in the vertical profile of the Indonesian Throughflow during Termination II: Evidence from the Timor Sea. *Paleoceanography*, *21*, PA4202. https://doi.org/10.1029/2006PA001278

Zhang, Y. G., Pagani, M., & Liu, Z. (2014). A 12-million-year temperature history of the tropical Pacific Ocean. *Science*, *344*(6179), 84–87. https://doi.org/10.1126/science.1246172

Zhang, Y. G., Pagani, M., & Wang, Z. (2016). Ring index: A new strategy to evaluate the integrity of TEX86 paleothermometry. *Paleoceanography*, *31*, 220–232. https://doi.org/10.1002/2015pa002848